Materials Science & Engineering C 100 (2019) 196–208

Contents lists available at ScienceDirect

Materials Science & Engineering C

journal homepage: www.elsevier.com/locate/msec

Bioactive diatomite and POSS silica cage reinforced chitosan/*Na*-carboxymethyl cellulose polyelectrolyte scaffolds for hard tissue regeneration

Sedef Tamburaci[a,b], Ceren Kimna[b], Funda Tihminlioglu[b,*]

[a] İzmir Institute of Technology, Graduate Program of Biotechnology and Bioengineering, Gülbahçe Campus, Urla 35430, İzmir, Turkey
[b] İzmir Institute of Technology, Department of Chemical Engineering, Gülbahçe Campus, Urla 35430, İzmir, Turkey

ARTICLE INFO

Keywords:
Diatomite
POSS
Na-carboxymethylcellulose
Chitosan
Scaffold
Silica

ABSTRACT

Recently, natural polymers are reinforced with silica particles for hard tissue engineering applications to induce bone regeneration. In this study, as two novel bioactive agents, effects of diatomite and polyhedral oligomeric silsesquioxanes (POSS) on chitosan (CS)/*Na*-carboxymethylcellulose (Na-CMC) polymer blend scaffolds are examined. In addition, the effect of silica reinforcements was compared with Si-substituted nano-hydroxyapatite (Si-Hap) particles. The morphology, physical and chemical structures of the scaffolds were characterized with SEM, liquid displacement, FT-IR, mechanical analysis, swelling and degradation studies. The particle size and the crystal structure of diatomite, POSS and Si-Hap particles were determined with DLS and XRD analyses. *In vitro* studies were performed to figure out the cytotoxicity, proliferation, ALP activity, osteocalcin production and biomineralization to demonstrate the promising use of natural silica particles in bone regeneration. Freeze-dried scaffolds showed 190–307 μm pore size range and 61–70% porosity. Both inorganic reinforcements increased the mechanical strength, enhanced the water uptake capacity and fastened the degradation rate. The nanocomposite scaffolds did not show any cytotoxic effect and enhanced the surface mineralization in osteogenic medium. Thus, diatomite and POSS cage structures can be potential reinforcements for nanocomposite design in hard tissue engineering applications.

1. Introduction

Biopolymer-based composites used in tissue engineering applications are named to be the new generation of high-performance materials by combining the advantages of inorganic materials and organic polymers such as flexibility, ductility, and processability [1].

Polysaccharide-based biopolymers have been widely used in biomedical applications. Their lower stability and faster degradation profile lead to use of crosslinkers, reinforcement agents or polymer blends to obtain required durable structure. Generally, chemical crosslinkers have limitations due to their possible toxicity for long term implantation. Among polysaccharide-based biopolymers, chitosan (CS) has been used as a scaffold material with its promoting effect on cell adhesion due its structural similarity to glycosaminoglycan groups and cationic nature at physiological pH. It can be widely preferred in various biomedical applications (drug delivery, cancer diagnosis, wound healing and tissue engineering) with its bioactivity, biodegradability and non-toxicity. Although chitosan is widely used as a scaffold material in bone tissue engineering applications, there is still necessity to improve its mechanical properties and degradation profile. Chitosan is highly degraded in the presence of lysozyme. This degradation behaviour is strongly related with its crystallinity and degree of deacetylation (DD) [2,3]. Polyelectrolyte complex scaffolds can be alternative to chemical crosslinkers that require usage of volatile organic agents. Polyelectrolyte complex formation is known as self-crosslinking between opposite charged polymer phases *via* electrostatic interactions. The PEC formation between oppositely charged polymers gains characteristic properties to final polymer blend in terms of solubility, swelling, and rheology. Cationic nature of chitosan permits its use with opposite charged natural polymers to form polyelectrolyte complexes (PECs) due to the ionic crosslinking between macromolecules [4]. *Na*-carboxymethyl cellulose (Na-CMC) is the only water-soluble derivative of cellulose which has distinctive properties with its opposite charge and structural similarity to chitosan. *Na*-carboxymethyl cellulose is physiologically harmless with high swelling capacity. Therefore, negatively charged *Na*-carboxymethyl cellulose can form polyelectrolyte complex

* Corresponding author.
E-mail address: fundatihminlioglu@iyte.edu.tr (F. Tihminlioglu).

https://doi.org/10.1016/j.msec.2019.02.104
Received 24 May 2018; Received in revised form 27 February 2019; Accepted 27 February 2019
Available online 01 March 2019
0928-4931/

with cationic chitosan that can mechanically improve the scaffold by acting as an ionic cross-linking agent [5,6]. The ionic cross linking between chitosan and Na-CMC was found to improve physical properties such as hydrophilic behavior, swelling degree and protein adsorption [7,8]. In a study, it was observed that polyelectrolyte complex scaffolds showed better cytocompatibility and higher proliferation rate when compared to pure chitosan [9]. CS/Na-CMC based scaffolds showed good biocompatibility, biodegradability and hydrophilicity which increased cell adhesion, spreading and proliferation [9,10]. In addition, it was reported that MG-63 and MSCs cells were attached and proliferated on n-HAP/CS/CMC composite scaffolds. Besides, it was supported with the *in vivo* study and confirmed that vascularization occurred in the porous structure during progressive degradation [11].

Scaffold designs for bone regeneration have focused on combining polymers with inorganic bioactive reinforcements to mimic the structure of bone tissue which is mainly composed of collagen matrix and hydroxyapatite. Nano-hydroxyapatite (HAP) has been generally incorporated into biodegradable polymers in succession because it is the main component of bone tissue as an inorganic phase [12–14]. The hydroxyapatite crystals provide calcium and phosphate ion source on the material surface which is substantial for cell differentiation and osteogenic cell proliferation [15]. Natural bone is composed of a non-stoichiometric apatite which contains trace elements such as Na, K, Mg, and Cl and they have essential importance in bone physiology. However, synthetic HAP nanoparticles do not resemble the inorganic part of natural bone tissue stoichiometrically that leads to problems in short-term osseointegration. Besides, HAP nanoparticles rapidly dissolve in body fluids, which leads to long term stability problem. Therefore, cations and anions are incorporated into HAP nanoparticles to improve the biological performance and overcome the dissolution and stability problem [16]. Silicon can be substituted into lattice phosphate sites of HAP to improve its biological activity and osseointegration [17].

Recently, silica-based nanoparticles came into prominence to induce bone tissue regeneration as an alternative to HAP crystals. Silica is the second most abundant biogenic mineral produced by various plants and animals [18]. Thus, it is revealed that the composites consisting biopolymers and silica particles have promising potential in biomedical applications. Silica incorporation supports cell adhesion by stimulating osteogenic proliferation through activating bone-related gene expression and enhancing the bone ingrowth as a calcifying agent. Besides, silica particles improve mechanical properties in the polymer structure. Studies showed that silica incorporation induced the CaO accumulation and nucleation of the apatite layer on the surface which are essential steps in hard tissue mineralization [19–21].

Among synthetic silica sources, polyhedral oligomeric silsesquioxanes (POSS) are the smallest synthetic silica particles which have silicon/oxygen cage inorganic part and organic hydrocarbon functional R groups attached to corner Si molecules [22,23]. POSS cages provide larger surface area compared with the microscale ceramic particles with its nanosized structure (1–3 nm). Stronger interfaces can be obtained with POSS incorporation in polymer matrix due to its nanosize [24].

Besides, POSS nanoparticles have covalently bonded functional R groups unlike conventional silica particles requiring surface modification. POSS molecules may exhibit a double role, comonomer and reinforcing agent with these R groups. Literature studies indicated that incorporation of POSS into polymer matrix *via* copolymerization or blending could significantly improve the properties of many polymers such as surface properties, glass transition, young' modulus and tensile strength. These enhancements were observed due to the good POSS–polymer matrix interactions [25,26]. POSS nanocages can be functionalized by changing its reactive R groups and that provides a strong interaction between POSS and polymer matrix. POSS nanoparticles have prominent characteristics such as cytocompatibility and non-toxicity [27]. Therefore, they can be used as nanofiller in biomedical applications as drug delivery systems [28]; cardiovascular [29,30], bone and dental nanocomposites [26,31,32].

As a natural silica source, diatom frustules are composed of hydrated amorphous silica cages, and used in many application areas such as filter aid, reinforcing filler and membrane due to their relatively low price and high abundance. Diatomite particles consist of silica mineral (88–90%) and a few other oxide components [33]. They have unique architectures; a porous structure which serves a large surface area and good mechanical properties with their amorphous silica skeleton [34,35]. Thus, they have been used as bioderived nanodevices and silica sources for biomedical applications (drug, gene delivery system, biosensor, and reinforcement agent) due to their unique microarchitecture [36–40].

Herein, the main objective of this study is to reinforce CS/Na-CMC polyelectrolyte complex scaffolds with two different novel silica sources; biosilica (diatomite) and hybrid silica nanocages (POSS) and to determine their effects on physical, mechanical and biological properties. In addition, these silica sources were compared with Si-substituted HAP particle which is commonly used as a reinforcing agent for bone tissue engineering. The scaffolds were prepared with freeze-drying technique and characterized with SEM, FT-IR, degradation, swelling study and mechanical test. The *in vitro* cytotoxicity, cell proliferation, ALP activity and mineralization were performed and compared with HAP incorporated scaffolds.

2. Material & method

Commercial low molecular chitosan (MW: 50–190 kDa, DDA %: 75–85) and Na-CMC (50–200 cP, 4% in H_2O at 25 °C) were purchased from Sigma-Aldrich and used for the preparation of scaffolds. Diatomite (Celatom FW-60 Eagle Picher Filtration & Mineral Inc., USA, 90% (w/w) silica), Si-substituted HAP nanopowder (Sigma-Aldrich, 5% (w/w) silica) and POSS Octa TMA® (Hybrid Plastics TM, 78% (w/w) Silica cage) were used as reinforcements. MG-63 cell line was supplied from Dr. Berivan Erik Cecen and SW1353 cell line was supplied from Prof. Dr. Leyla Didem Kozaci. Minimum essential medium (MEM, Sigma-Aldrich), fetal bovine serum (FBS) penicillin-streptomycin solution and L-glutamine (Lonza) were used for cell culture studies. WST-1 ready to use cell proliferation reagent (BioVision Inc.), LDH Cytotoxicity Assay Kit (Pierce, Thermo Scientific), Resazurin Cell Viability Kit (Cell Signaling Technology Inc.) and ALP-Enzyline PAL optimise kit (Biomerieux Inc.) were used for *in vitro* assays. Silver nitrate and sodium thiosulfate (Sigma, Aldrich) were used for von Kossa staining. Alizarin Red S (Sigma, Aldrich) was used for Alizarin Red staining protocol.

2.1. Scaffold preparation

Before use, HAP, POSS and calcined diatomite particles were dried at 80 °C for 24 h to remove the moisture and prevent the agglomeration. Firstly, 1% w/v LMW chitosan and 1% w/v Na-CMC aqueous solutions were prepared separately. 10% w/v inorganic additives (POSS, Si-HAP, calcined diatomite) were dispersed in distilled water with continuously stirring for 24 h. Then, polymer solutions and inorganic aqueous dispersions were mixed under vigorous stirring to obtain reinforced polymer blend. Finally, acetic acid (1% *v*/v) was added dropwise to the polymer solution. The homogeneous mixtures were poured into well-plates and prefreezed at −20 °C for 24 h and lyophilized. Scaffolds were stored in a desiccator for further use.

2.2. Characterization tests

2.2.1. Morphology

Composite scaffolds were analyzed with Scanning Electron Microscopy (SEM) to observe the surface morphology and average pore sizes. Microscopic view of inorganic fillers was observed with SEM analysis. In addition, STEM and AFM analyses were performed to observe the morphology of POSS and Si-HAP nanoparticles. Nanoparticles

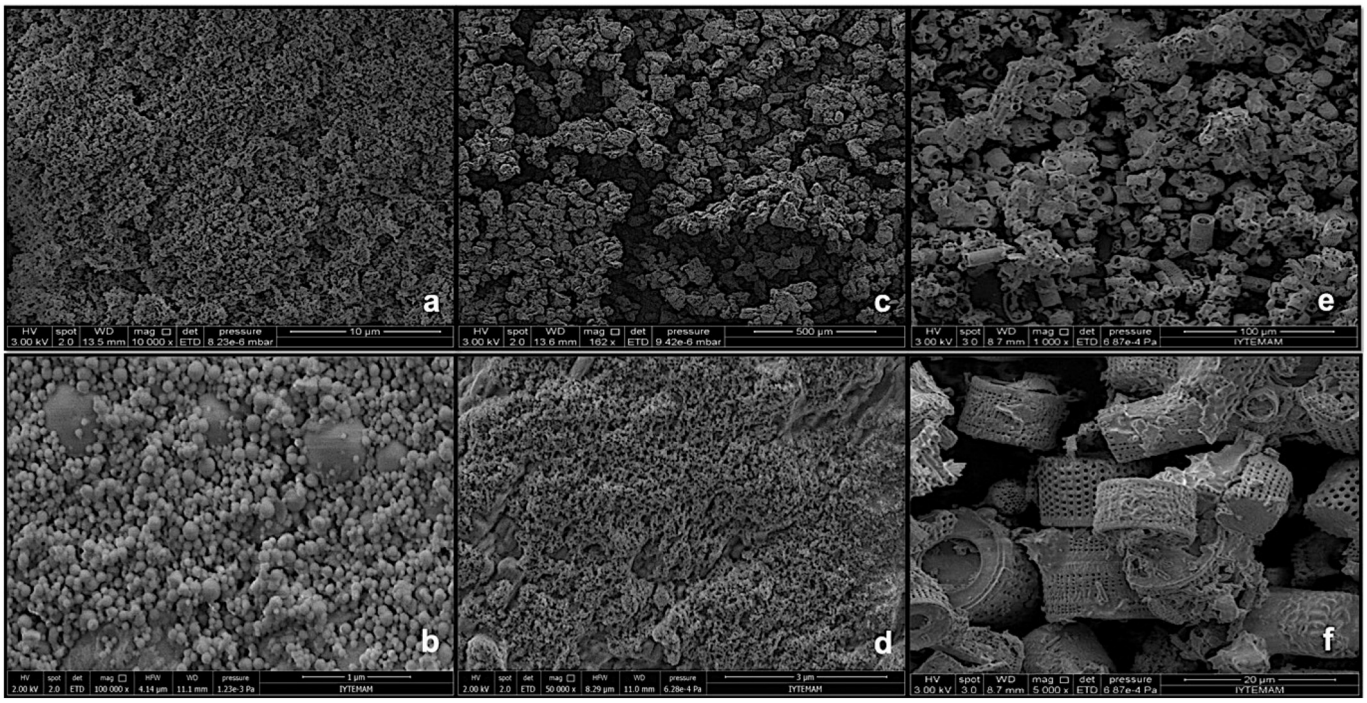

Fig. 1. SEM images of HAP (a), POSS (b) and diatomite (c) particles.

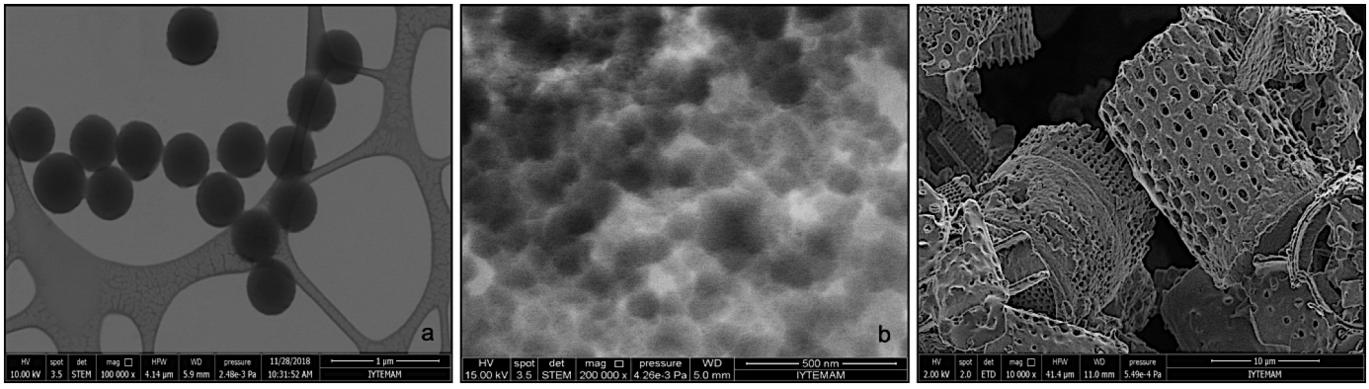

Fig. 2. STEM images of Si-HAP and Octa-TMA POSS nanoparticles dispersions on copper grids and SEM image of diatomite particles.

were dispersed in ultrapure water with 10^{12} dilution factor. Nanoparticle dispersions were dripped on TEM grids (Ted Pella 400 mesh copper grid supported with ultrathin carbon film) and coverslips. Before SEM analysis, samples were coated with a thin gold layer under Argon gas by using Emitech K550X. The analysis was performed with Quanta FEG 250 (at 7×10^{-2} mbar and 15 mA). Image J software was used to calculate the average pore sizes. DLS Analysis was performed in a Malvern Zeta-sizer Nano ZS to determine the hydrodynamic sizes of the inorganic fillers. 1% w/v of dispersions were prepared with deionized water and incubated in an ultrasonic bath for 5 min before testing.

2.2.2. Open porosity measurement

The open pore percentages of the composite scaffolds were determined with the liquid displacement method [41]. Scaffolds (n = 3) were immersed in a graduated cylinder with a known volume (V_1) of ethanol. The cylinder is placed in a vacuum to force the ethanol into the pores of the scaffold until no air bubble emerged from the scaffold. The total volume of the ethanol and scaffold is then recorded as V_2. The volume difference ($V_2 - V_1$) is the volume of the skeleton of the scaffold. Then, the scaffold is removed from the ethanol and the residual ethanol volume is measured as V_3. The porosity of the open pores in the scaffold is evaluated with the Eq. (1).

$$\varepsilon = (V_1 - V_3)/(V_2 - V_3) \quad (1)$$

2.2.3. X-ray diffraction (XRD) analysis

XRD analysis was performed to observe the crystal structure of each reinforcement group. X-ray diffraction patterns of inorganic filler powders were determined at a voltage of 40 kV using Cu-Kα radiation (λ = 1.54 Å). Intensities were recorded in a range of 5–60° (2θ) with a scanning rate of 0.139°/s (Philips X'PertPro).

2.2.4. Fourier transform infrared spectroscopy (FT-IR) analysis

The chemical structure of the samples and the silica incorporation to the polymer blend were analyzed by a Fourier Transform Infrared Spectroscopy (FT-IR) using ATR attachment (Shimadzu FTIR-8400S) at wavelengths ranging from 4000 to 650 cm^{-1} at a resolution of 4 cm^{-1}.

2.2.5. Mechanical analysis

The mechanical strength of the scaffolds was measured by compression test according to the ASTM-D 5024-95a Standard with TA XT

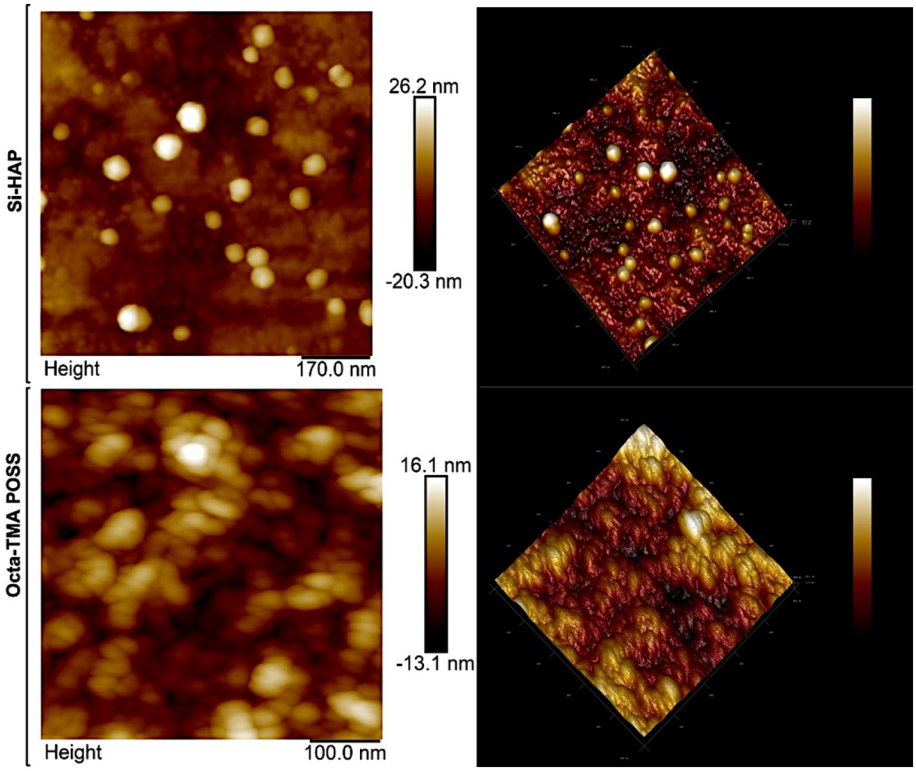

Fig. 3. AFM phase and topography images of Si-HAP and Octa-TMA POSS nanoparticle dispersions.

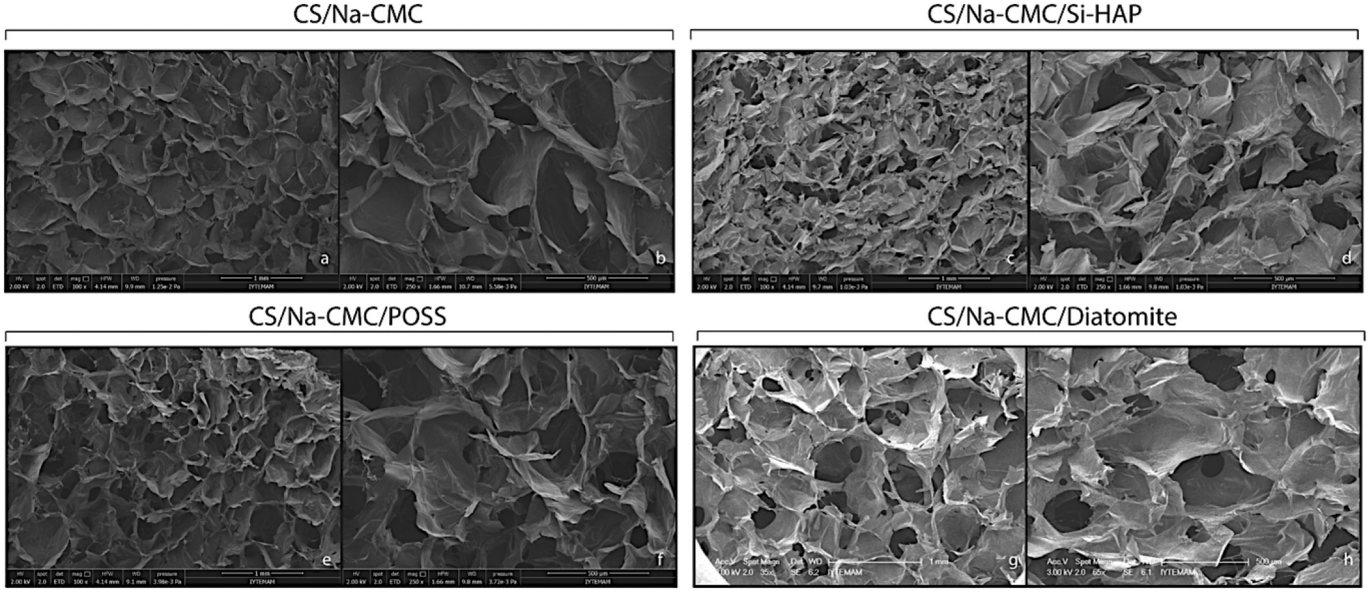

Fig. 4. SEM images of CS/Na-CMC (a, b); Si-HAP (c, d); POSS (e, f); and diatomite (g, h) incorporated CS/Na-CMC scaffolds, respectively.

Table 1
Average pore sizes and porosity % values of scaffolds.

Analyses	SEM	Liquid displacement
Groups	Average pore size (μm)	Porosity (%)
CS/Na-CMC	266 ± 15	61 ± 8.0
CS/Na-CMC 10% HAP	307 ± 30	70 ± 3.8
CS/Na-CMC 10% POSS	190 ± 16	70 ± 3.8
CS/Na-CMC 10% diatomite	239 ± 20	68 ± 2.6

Plus Texture Analyser (Stable Micro Systems). Compression was applied with ½″ cylindrical Delrin probe, a cross-head speed of 5 mm/min at room temperature and compressed up to 50% of scaffold's original height. Average mechanical compression data of five test specimens were determined with standard error.

2.2.6. Swelling study

Swelling test was performed in order to obtain water uptake capacity of scaffolds. Samples (n = 3) were stabilized with immersing into 100% ethanol solution then dried at room conditions. Dry scaffolds were weighted and then wetted with Phosphate Buffer Saline (PBS)

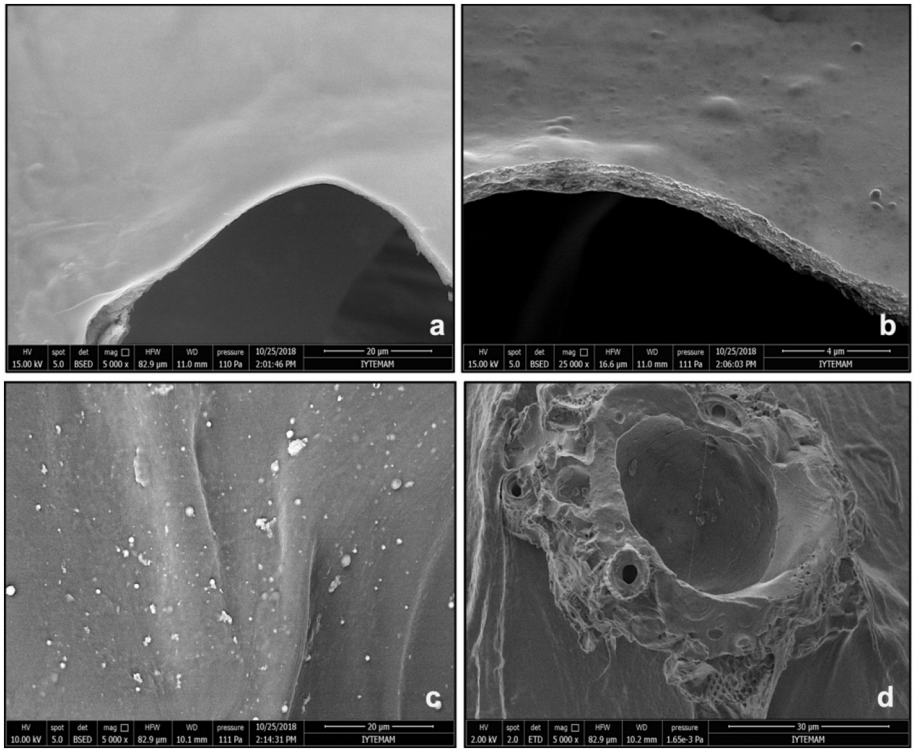

Fig. 5. SEM images of Si-HAP, POSS and diatomite particles dispersed in CS/Na-CMC matrix: CS/Na-CMC control (a); POSS (b); Si-HAP (c); diatomite (d).

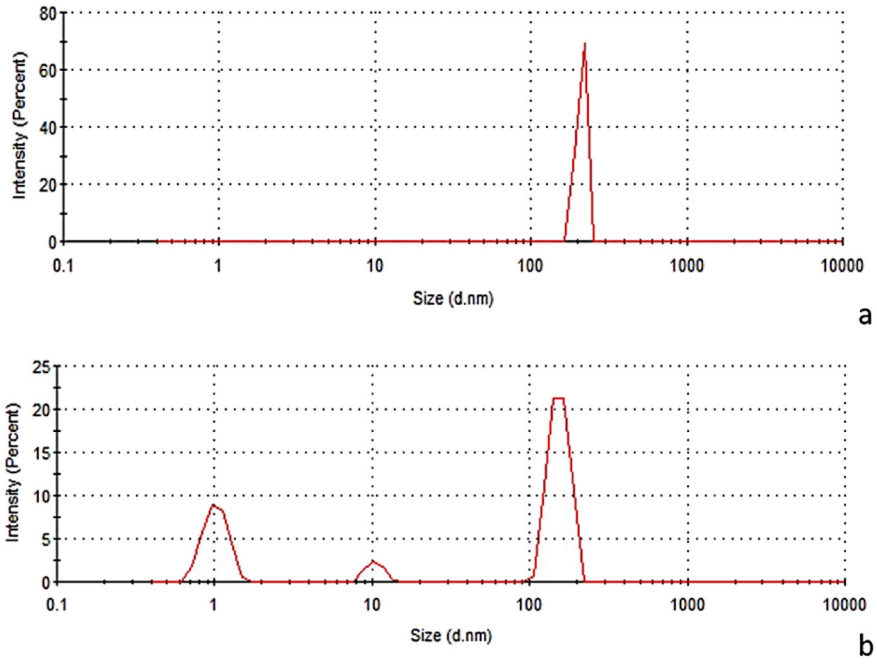

Fig. 6. Hydrodynamic sizes of Si-HAP (a) and POSS (b) particles.

solution (pH = 7.4). Wet samples are weighted after 24 h of incubation. Swelling % is calculated with Eq. (2) shown below:

$$\text{Water uptake capacity}\ (\%) = ((W_s - W_d)/W_d) \times 100 \quad (2)$$

where; W_s and W_d are the swollen and dry weight of samples, respectively.

2.2.7. Enzymatic degradation

Phosphate-buffered solution (PBS, pH = 7.4) containing 1.5 μg/mL lysozyme (from chicken egg white-Sigma Aldrich) was used as degradation medium and refreshed in every 48 h to obtain sustained enzyme activity. 0.01% w/v sodium azide (Sigma Aldrich) was added to the solution in order to prevent the bacterial contamination. Weight loss % of samples (n = 3) were investigated for 7 and 21 days of incubation. The experiments were conducted thrice and the weight loss % in degradation process was calculated according to the Eq. (3).

$$\text{Weight Loss}\% = ((\text{Initial weight} - \text{Dry weight})/\text{Initial weight}) \times 100 \quad (3)$$

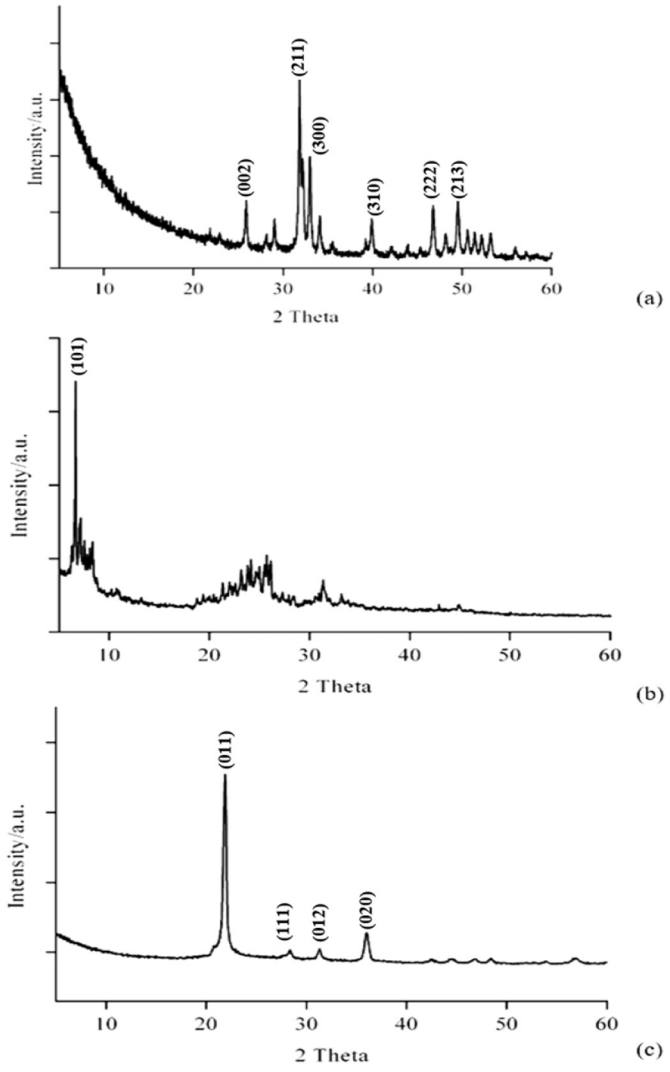

Fig. 7. XRD patterns of Si-HAP (a), POSS (b) and diatomite (c) particles.

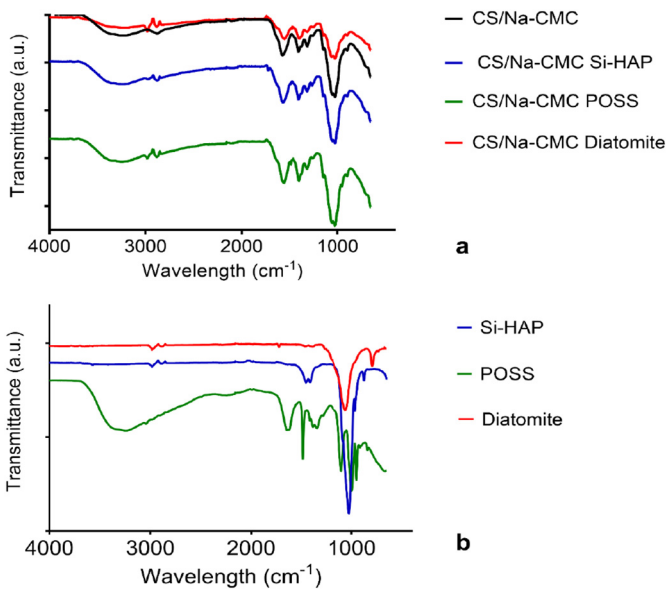

Fig. 8. FT-IR spectra of silica incorporated CS/Na-CMC scaffolds (a) and Si-HAP, Diatomite and POSS particles (b).

2.3. *In vitro* cell culture studies

Scaffolds were sterilized by incubation in 70% EtOH solution. MG-63 and SW1353 cell lines were used for *in vitro* studies.

2.3.1. *In vitro* cytotoxicity determination

In vitro cytotoxicity assay was performed with the indirect extraction method according to ISO-10993 standard. Scaffolds (n = 3) were extracted for 24 h in MEM at 37 °C and used as an incubation medium. Cell seeding was carried out at 10^5 cell/ml cell density and incubated on 96-well plates. MG-63 and SW1353 cell lines were used to investigate the cell viability for bone and bone-cartilage interface. The viability % of MG-63 and SW1353 cells were evaluated by the WST 1 assay. The cytotoxicity of the scaffolds was measured by spectrophotometrically at 440 nm in 24, 48 and 72 h of incubation periods. The cell viability is calculated with the Eq. (4).

$$\text{Cell viability\%} = (\text{Absorbance of sample}/\text{Absorbance of NC}) \times 100 \quad (4)$$

where NC is the negative control.

2.3.2. Cell proliferation assay

Cell proliferation on scaffolds was determined by using Resazurin Cell Viability kit (Biovision Inc.). MG-63 cells were seeded at a density of 2.5×10^6 cell/scaffold in 24-well plates and incubated for 10 days. Cell proliferation was observed at 7 and 10 days of incubation with the rezasurin assay and quantified by measuring the relative fluorescence units (RFU) using a fluorescence plate reader (Varioskan Flash) at 530–570 nm excitation and 590–620 nm emission (n = 3). Concerning the cell membrane integrity, lactate dehydrogenase (LDH) assay was also used to determine the possible cytotoxic effect of silica incorporation on cell culture during proliferation with LDH Cytotoxicity Assay Kit (Pierce, Thermo Scientific). The release of LDH activity in the supernatants of the culture medium was measured at 490 nm.

2.3.3. Alkaline phosphatase (ALP) activity and osteocalcin (OC) production

The alkaline phosphatase production of cells on scaffolds was evaluated by ALP-Enzyline PAL optimize kit (Biomerieux Inc.) MG-63 cells were seeded at a density of 2.5×10^6 cell/scaffold and cultured with osteogenic medium. ALP activities of cells were quantified by colorimetric ALP kit at 7 and 14 days of incubation periods. The absorbance of the medium was measured by a plate reader (Varioskan Flash) at 405 nm (n = 3). Osteocalcin (OC) production of MG-63 cells cultured on scaffolds was measured using Sandwich-ELISA assay (Human OC/BGP (Osteocalcin) ELISA Kit, Elabscience). Osteocalcin concentrations were analysed with culture media extracted from scaffolds for 21th and 28th days of culture.

2.3.4. *In vitro* mineralization with von Kossa and Alizarin Red staining

After 14 days of incubation, MG-63 cells were fixed with 3.7% paraformaldehyde for 20 min at room temperature, washed with 1× PBS solution. Phosphate deposition was determined with von Kossa staining method. Scaffolds stained with 1% (w/v) aqueous silver nitrate solution were incubated under UV light in laminar flow cabinet for 30 min. Then, scaffolds were incubated with 5% w/v sodium thiosulfate solution to remove unreacted silver to detect a yellow-brownish stain. Calcium deposition was determined with Alizarin Red S staining. The calcium ions precipitate with alizarin stain and the deposits turn into the red at once [42]. Scaffolds were observed under stereomicroscope (SOIF DA 0737). Furthermore, quantification of ARS was done according to the literature [43]. The absorbance of the solubilized stain was measured at 405 nm. Data were presented as ± standard error (n = 3).

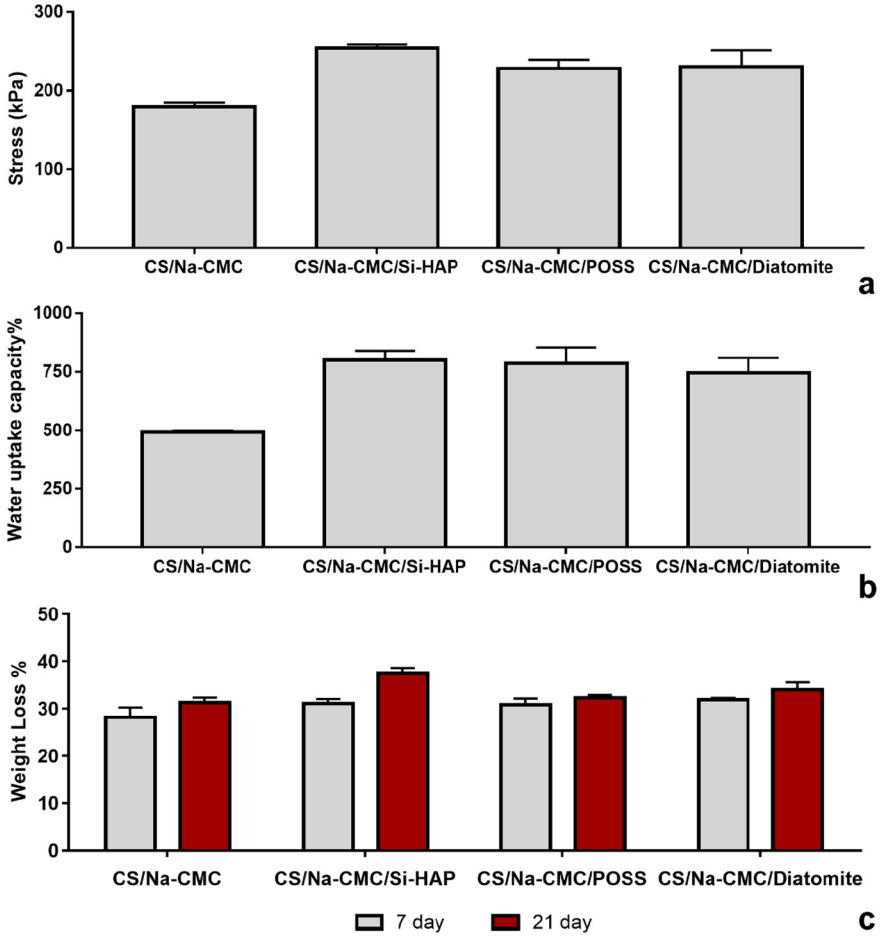

Fig. 9. Mechanical strength (a), water uptake capacity (%) (b) and weight loss % (c) of control (CS/Na-CMC), HAP, POSS and diatomite reinforced composite scaffolds.

2.4. Statistical analysis

All experiments were repeated thrice, and the experimental data are expressed as the mean ± standard error deviation (SED). Characterization test results were evaluated with the one-way analysis of variance (ANOVA, $P < 0.05$). Statistical analyses of *in vitro* studies were carried out using two-way analysis of variance (ANOVA, $P < 0.05$).

3. Results and discussion

3.1. Morphology

Surface topography is an important factor that alters cell adhesion and spreading on biomaterial surface. These alterations are directly related with size and morphology which significantly affect the bioactivity of particles that are incorporated in polymer matrix. Silica particles alter the surface roughness of polymer matrix as well as providing osteogenic effect in bone tissue regeneration [44,45]. Diatomite, Si-HAP and Octa-TMA POSS nanoparticles were observed with SEM analysis. Morphology of Si-HAP, POSS and diatomite particles were shown in Fig. 1. POSS and Si-HAP inorganics were observed as agglomerated nanoparticles. It was found that the calcined diatomite particles used in the study are dominantly composed of *Melosira granulata* species. Although these frustules have microstructures, they showed nanotopographies with their nanoscale channels and pore sizes. Morphological features of POSS and Si-HAP nanoparticles were indicated in detail with STEM analysis (Fig. 2). STEM images showed that Si-HAP nanoparticles exhibited spherical morphology with uniform distribution whereas POSS nanoparticles were observed as granular agglomerations. AFM images of nanoparticles revealed that Si-HAP nanoparticles were dispersed effectively with spherical morphology (Fig. 3). However, granular POSS nanoparticles showed tendency to form clusters and aggregations with each other due to the strong interactions between their active R groups.

Microstructure and the average pore sizes of scaffolds were investigated with SEM analysis (Fig. 4). The average pore sizes and the porosity % values of the scaffolds were depicted in Table 1. SEM images showed that highly interconnected, porous CS/Na-CMC polyelectrolyte scaffolds were successfully fabricated by the freeze-drying method. As seen in Table 1, average pore sizes of the scaffolds were found to be in a range of 190–307 μm. CS/Na-CMC scaffolds as control group exhibited an average pore size of 266 ± 15 μm. In general, inorganic fillers did not show a significant effect on morphology because of their relatively small concentrations in the polymer blend. However, particle size differences from micro to nano-level affects the dispersion level which alters altering polymer matrix structure. Incorporation of POSS nanocages and diatomite particles slightly decreased the pore size as 190 and 239 μm, respectively whereas Si-HAP nanoparticles increased the pore size slightly. These differences may arise from the distribution level of particles in polymer matrix. Besides, particle incorporation affects the viscosity of polymer blend which is an important factor for pore formation in freeze-drying method. In our study, minimum pore sizes were observed in POSS incorporated group which may be attributed to dispersion of POSS particles which possess smallest size compared to Si-HAP and diatomite particles. In addition, it arises from viscosity

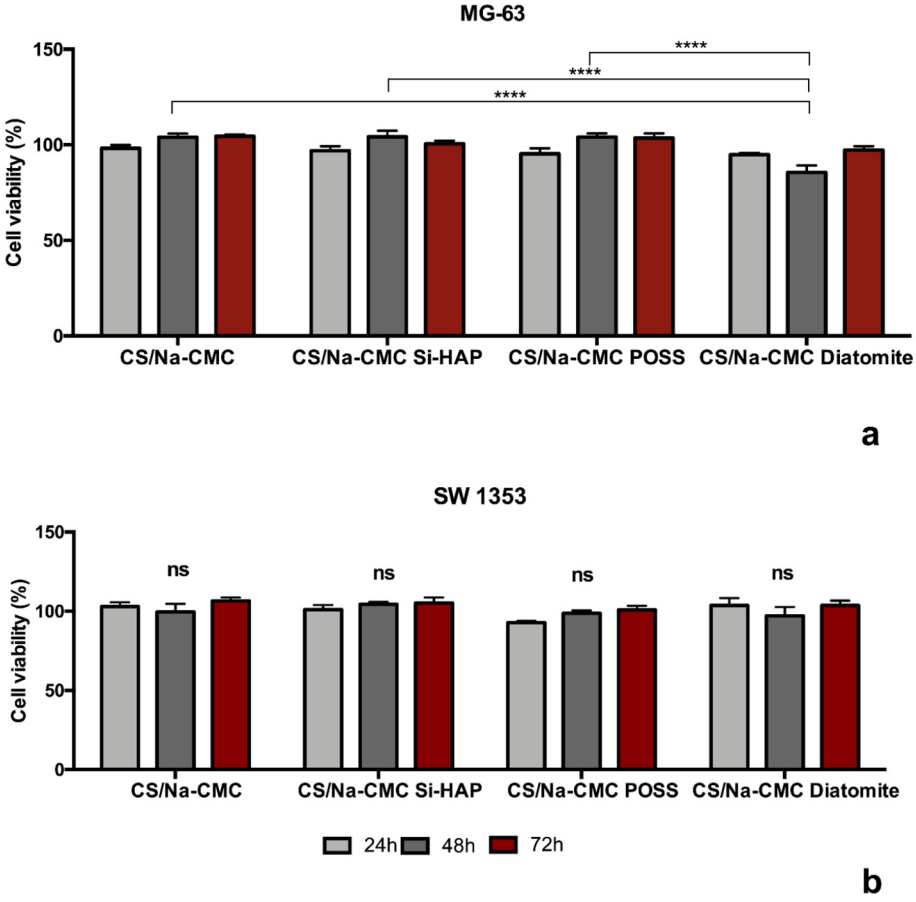

Fig. 10. MG-63 (a) and SW1353 (b) cell viability % measured with WST-1 assay.

diminishing effect of POSS in polymeric solutions [46] as found by Whang et al. in PLGA scaffolds [47].

On the other hand, maximum average pore size was observed on Si-HAP incorporated scaffolds as 307 ± 30 μm due to the small agglomerations of Si-HAP nanoparticles in polymer matrix. These agglomerations may affect the dispersion level of Si-HAP nanoparticles in polymer matrix and morphology of pore walls in porous scaffolds. All groups had the required minimum pore size of 100 μm which is critical for the diffusion of nutrients and oxygen for cell survival [48]. Besides, pore size range of 200–350 μm was found to be optimum for cell proliferation and vascularization in bone tissue engineering [49]. Consequently, prepared CS/Na-CMC scaffolds have convenient pore sizes for tissue regeneration.

According to the liquid displacement study, the porosity of the scaffolds was found as 61–70%. The inorganic reinforcements slightly increased the porosity by changing the viscosity of polymer blend. This effect may lead to forming of more interconnected pores in the structure. The porosity percentage of composite scaffolds is found to be appropriate to allow cell migration and nutrient supply to mimic the trabecular bone which has a porosity range between 50 and 90% [50].

SEM analysis was also performed to investigate the distribution of particles in CS/Na-CMC matrix. SEM images showed that Si-HAP nanoparticles and diatomite frustules were physically dispersed and attached on scaffold surface by showing good interaction with polymer blend. Diatomite frustules are highly porous silica particles with high permeability and low density. Thus, they are dispersed in polymer matrix effectively with their unique microarchitecture. On the other hand, POSS nanoparticles were embedded in polymer matrix due to the possible interaction of their methyl ammonium R groups with polymer blend (Fig. 5).

According to the DLS results (Fig. 6), it was found that Si-HAP nanoparticles possessed hydrodynamic sizes of 168 nm by means of their intensity size distribution. Non-aggregated POSS nanocages (30%) were observed with an average size around 1 nm similarly as indicated in the literature [27]. It was observed that most of the POSS particles (higher than 64.8%) were found as aggregated forms (153 nm) due to their strong interaction between their reactive groups. The solution comprised of small aggregations (5%) having an average size of 10.42 nm in accordance with the findings in the literature [51]. The diatomite particles showed particles over working range of DLS, therefore, they could not be characterized in terms of their hydrodynamic sizes (Fig. 6). Therefore, SEM micrographs were used with Image J software to determine the average particle size of the diatom frustules. According to the SEM images, diatomite particles had an average diameter of 10.88 ± 0.7 μm with a pore size of 496 ± 40 nm.

3.2. X-ray diffraction (XRD) analysis

Fig. 7 shows the XRD spectra of the HAP, POSS and Diatomite particles with Bragg's angle (2θ) varying from 5° to 60°. The average crystallite sizes were determined by Scherrer analysis of diffraction peaks [52]. Crystallite size of hexagonal HAP was found as 40 nm according to 2θ = 25.92° (Fig. 7a) since HAP inclines to grow in the c-axis that corresponds to (002) reflection peak [53]. The XRD profile of POSS nanoparticles confirmed the crystalline structure, with a characteristic diffraction peak at 2θ values of 6.65°, 10.79° and 18.76° [54–56]. Estimation of the average crystallite size was done by using the average widths of the strongest reflections and found as in the range of 70 nm (Fig. 7b). A higher value of the crystallite size for POSS could be due to the contribution of ligand groups on the crystals structure of POSS as well as agglomerations of the nanoparticles that lead to larger crystallite sizes [56–58]. Diatomite particles showed crystalline cristobalite

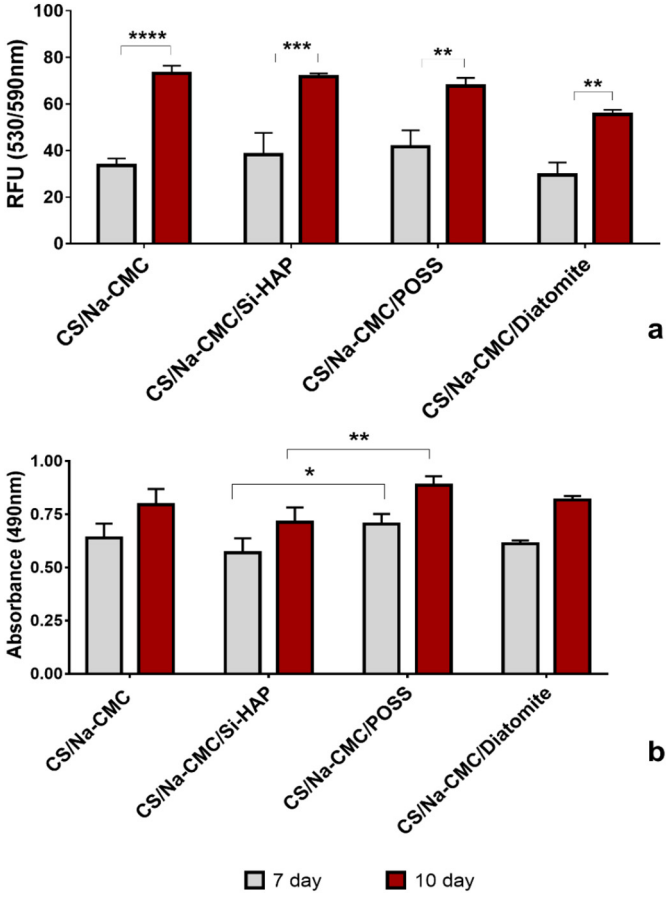

Fig. 11. MG-63 proliferation on scaffolds and LDH activity of MG-63 cells during proliferation (b).

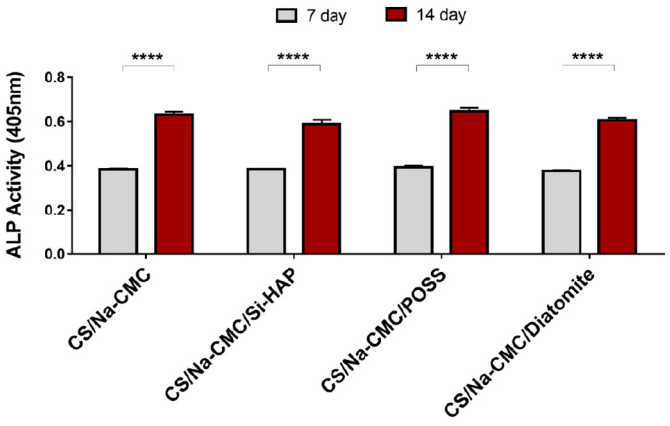

Fig. 12. ALP Activity of MG-63 cells cultured on scaffolds for 7 and 14 days.

silica peaks according to its Opal C structure which is a well-ordered form of the silicate [59]. According to Scherrer equation, the average crystallite size of tetragonal diatomite was found as 48 nm by using most intense peaks (Fig. 7c).

3.3. Fourier transform infrared spectroscopy (FT-IR) analysis

FT-IR spectral analysis of the samples was performed to confirm the strong ionic interactions between NH_2 groups of CS and –COO groups of Na-CMC which forms the polyelectrolyte complexes (Fig. 8a). In our previous study, basic characteristic peaks of chitosan; NH_2 bending at 1600–1635 cm^{-1}, N—H bending at 1580 cm^{-1} and NH stretching at

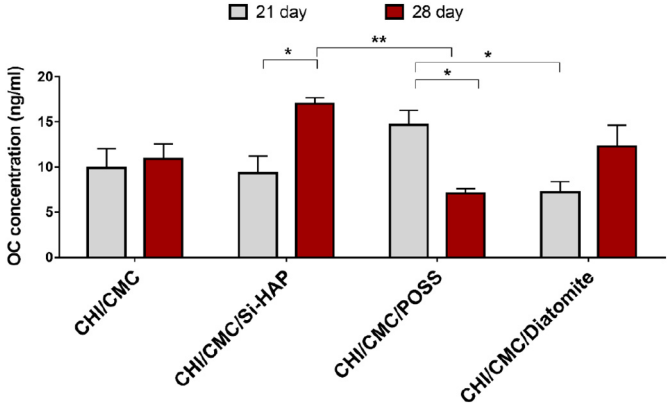

Fig. 13. Osteocalcin secretion of MG-63 cells cultured on scaffolds for 21 and 28 days.

3000–2500 cm^{-1} were detected. Stretching vibrations of OH groups of chitosan were determined in the range of 3547–2850 cm^{-1} [40]. Similarly, the band caused by stretching vibrations of OH groups was seen in 3000–3620 cm^{-1}. The characteristic CMC peak due to > CH-O-CH_2 stretching was found at the wavelength of 1052 cm^{-1} [60]. The polyelectrolyte complex caused by cationic CS and anionic Na-CMC interaction was depicted with the presence of a band at 1562 cm^{-1}. Our result is in good agreement with the band regarding polyelectrolyte complex formation reported in the literature at 1589 cm^{-1} [61]. The broad peak at a wavelength of 2850 cm^{-1} due to C—H stretching bonds at the control group transformed into two sharp peaks at 2860 and 2930 cm^{-1}. The spectra results show that the pure TMA-POSS shows a strong and symmetric Si—O—Si stretching absorption band at 1070 cm^{-1} was assigned to Si—O—Si asymmetric stretching as the characteristic absorption peak of silsesquioxane inorganic cages (Fig. 8b). The peak at 920 cm^{-1} was attributed to the torsional vibration of NMe_4 groups in POSS structure as found at the wavelength of 936 cm^{-1} in the literature [62]. Diatomite particles show characteristic absorption at 1070 cm^{-1} that are assigned to Si—O—Si stretching. The FT-IR results indicated that cationic chitosan and anionic Na-CMC provided a polyelectrolyte complex. Also, results showed that silica sources were incorporated into polymeric blend successfully.

3.4. Mechanical analysis

Scaffolds should have similar mechanical properties at the defect side in bone regeneration to supply the mechanical integrity. Chitosan and cellulose show low mechanical properties with their natural polymeric structures. Polyelectrolyte complexes generally overcome this limitation by forming ionically crosslinked stable structure. In addition, inorganic reinforcements are preferred to overcome the mechanical disadvantage of polymeric scaffolds in bone tissue engineering applications as well as enhancing bioactivity. Therefore, silica particles were used to reinforce CS/Na-CMC polyelectrolyte blend to enhance the mechanical properties as well as inducing surface bioactivity. Si-HAP reinforced CS/Na-CMC scaffolds were used to compare the effect of silica particles with the HAP crystals mainly found in the bone structure. Mechanical properties of dry scaffolds were determined by compression test and depicted in Fig. 9a. In comparison to control group (179.3 kPa), both diatomite particles (230.3 kPa) and POSS nanocages (228 kPa) enhanced the mechanical strength reinforcing the structure of CS/Na-CMC polyelectrolyte blend. Si-HAP incorporated scaffolds showed the maximum mechanical strength (254.3 kPa) according to the intermolecular hydrogen bond and possible chelation with chitosan. The differences among groups were found to be statistically significant ($P < 0.05$).

The desirable compressive strength of Si-HAP incorporated scaffolds

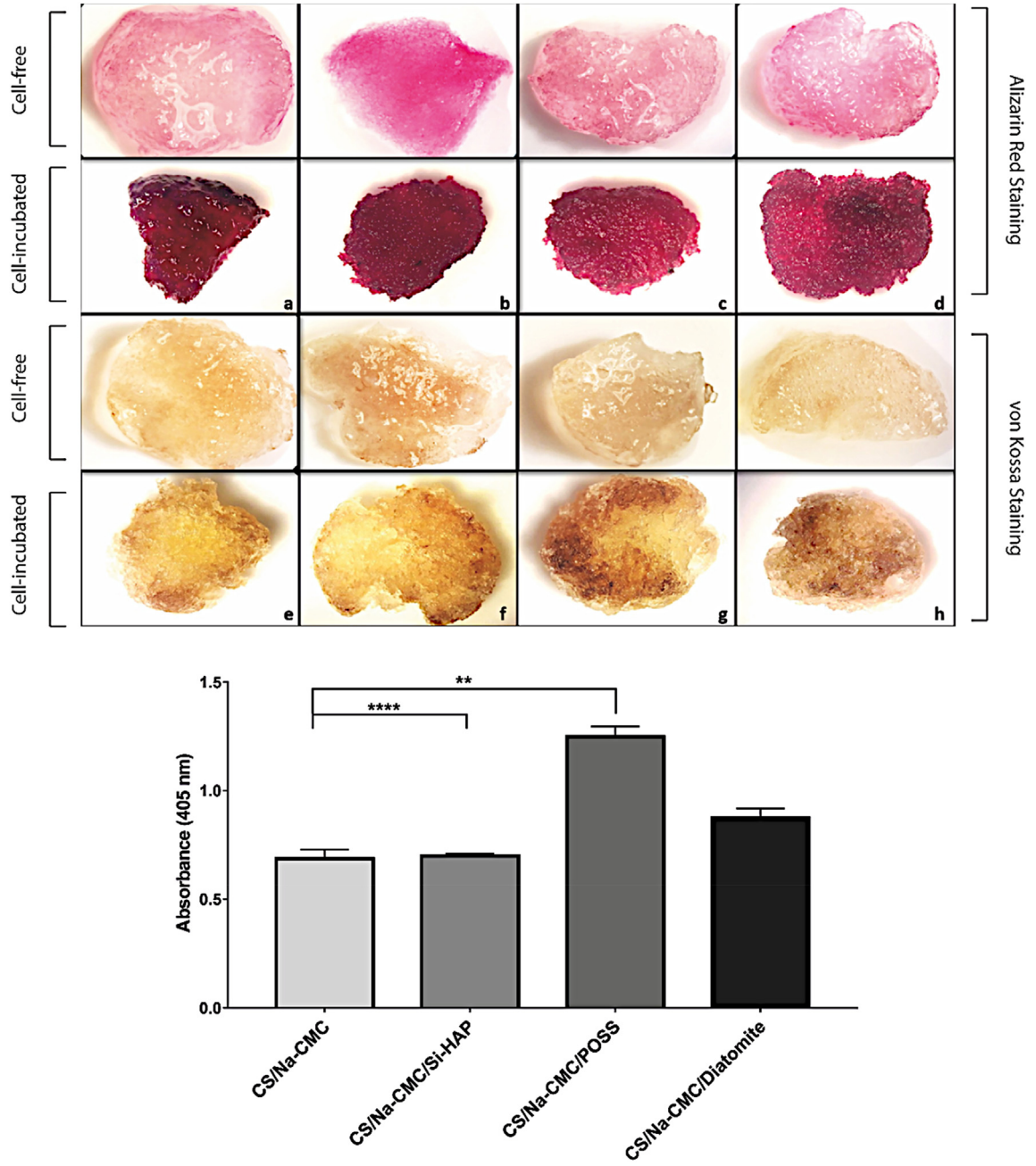

Fig. 14. Stereomicroscopy images of Alizarin Red and von Kossa staining on control (a, e) and Si-HAP (b, f); POSS (c, g); diatomite (d, h) incorporated scaffolds at 14 days, respectively. Semi-quantification of Alizarin Red S staining by absorbance at 405 nm.

can be attributed to the possible interactions of Ca^{2+} and PO_4^{3-} on hydroxyapatite surface and the polymer matrix. Besides, diatomite and POSS particles incorporated into the polymer blend successfully and reinforced the structure with their nanotopographic features. It is known that nanosized particles formed a tighter interface with polymer blend due to their large surface area [63]. This effect was proven in our previous studies [26,40]. Both POSS nanoparticles and diatomite frustules formed a good interface with CHI/Na-CMC blend polymer matrix. Therefore, mechanical properties were enhanced due to the hydrophilic nature and nanotopographic morphology of the silica particles that are compatible with the hydrophilic polymer matrix.

3.5. Swelling study

Water uptake capacity % values of scaffolds were illustrated in Fig. 9b. Silica incorporated scaffolds showed higher water uptake capacity than the control group according to the hydrophilic nature of the silica sources. Also, the water uptake capacity is related to the higher porosity of the composite scaffolds having more vacant sites [64]. Si-HAP, POSS, and diatomite containing scaffolds had 799.9, 785.5, and 745.5% water uptake capacity at 24 h of incubation, respectively. Therefore, it can be said that Diatomite and POSS incorporated scaffolds showed similar water uptake capacity with the Si-HAP loaded scaffolds. Thus, the hydrophilic nature of the fabricated scaffolds can allow nutrient diffusion by absorbing the body fluid. The differences among groups were found to be statistically significant ($P < 0.05$).

3.6. Enzymatic degradation

In the degradation study, CS/Na-CMC scaffolds decomposed

enzymatically in the presence of lysozyme. *In vitro* biodegradation profile of scaffolds was determined for 7 and 21 days of incubation (Fig. 9c). Silicate-based nanoparticles generally enhance water uptake capacity of the polymer matrix. This affects the degradation behavior of the polymer by modifying its surface and bulk properties and accelerates the degradation process of the composite [65]. Therefore, the material absorbs more water leading the hydrolytic attack in the structure. All groups showed slightly higher degradation rate compared to control group. The weight loss % of silica incorporated scaffolds slightly increased at the 21 day of incubation due to the possible dissolution of silica particles from the scaffold surface compared to control. The increasing trend with the addition of silica sources could be attributed to ion exchange and the hydrolysis of Si-O-Si bonds disintegrating the network in the aqueous media [66–68]. At the end of the 21st day, 31.3 wt% of control group degraded while POSS and diatomite incorporated scaffolds had a weight loss % of 32.3 and 34, respectively. Maximum weight loss % was obtained for Si-HAP incorporated scaffolds with 37.5%. Si substitution to HAP also increased the solubility of the particles [69]. However, diatomite and POSS composite scaffolds degraded more slowly compared to the Si-HAP composite scaffolds due to their cage structures and possible stronger interaction within the polymer matrix.

3.7. In vitro studies

3.7.1. Cytotoxicity determination

Cytotoxicity of scaffolds on MG-63 and SW1353 cells was evaluated by 24 h extraction of scaffolds in 24, 48 and 72 h of incubation periods and depicted in Fig. 10(a, b). The results were reported for control and 10 wt% silica reinforced CS-Na-CMS composites and compared with the 10 wt% Si-HAP reinforced composites. It is noted that nano silica incorporation did not cause any toxic effects on MG-63 cells seeded on chitosan-based scaffolds [70]. Our previous study results showed that diatomite incorporation to neat chitosan matrix did not show any cytotoxic effect on Saos-2 human osteosarcoma cell line [40]. Microscale morphology of the diatomite showed a negative effect on MG-63 cell monolayer causing a non-significant decrease at a 48 h, followed by an increase in 72 h. This may stem from the effect of particle size on cell-material interaction [71]. Since dissolution of silicate groups from scaffold is expected during indirect extraction process, it may affect adversely cell bioactivity due to the direct contact with cell monolayer. However, in this study, *in vitro* cytotoxicity assay indicated that both types of silica, as well as Si-HAP incorporation to CS/Na-CMC scaffolds with 10% loading, did not show any cytotoxic effect on both human osteosarcoma MG-63 and chondrosarcoma SW1353 cell lines. SW-1353 cell line was used to investigate the possible effects on bone-cartilage tissue interface. Thus, these results conclude that the diatomite and POSS particles with 10% w/v concentration could be used to enhance the bioactivity of polymeric scaffolds as an alternative to HAP for hard tissue engineering applications.

3.7.2. Cell proliferation study

The MG-63 proliferation on silica incorporated CS/Na-CMC scaffolds was determined with resazurin assay for 7 and 10 days of the incubation period (Fig. 11a). Cell proliferation on each group significantly increased by incubation time ($P < 0.05$). Maximum cell proliferation was obtained on Si-HAP composite scaffolds whereas minimum cell proliferation was observed diatomite incorporated scaffolds. However, results showed that MG-63 osteoblast-like cells proliferated on scaffolds successfully and silica incorporation did not reveal a remarkable effect on cell proliferation. LDH activity results showed that POSS and diatomite incorporations had similar effects on cells compared to control scaffold group. LDH activity slightly increased during incubation period and silica incorporation did not show any significant cytotoxicity to MG-63 cells cultured on scaffolds (Fig. 11b).

3.7.3. Alkaline phosphatase (ALP) activity and osteocalcin secretion

ALP activity determination was used to observe the effect of silica particles on osteoblast differentiation at the early stage of bone regeneration. ALP is known as a marker factor for differentiation of osteoblasts for bone regeneration. ALP was postulated to increase the local concentration of inorganic phosphate [72,73]. Recent studies revealed that, silica particles enhance the bioactivity of osteoblasts and stimulates their responses by inducing the differentiation markers especially enhancing biomineralization [74–77]. These osteogenic effects are strongly related with particle size and morphology. These factors alter the surface topography and enhance osteoblast-material interaction in bone regeneration [45]. Fig. 12 shows the ALP activity of the MG-63 cells on scaffolds for 7 and 14 days of incubation. All composite groups had similar increasing ALP activity trend during the incubation period in osteogenic medium. Increase in ALP activity by incubation time was found to be statistically significant ($P < 0.05$) for all groups. Maximum ALP activity (0.603) was observed on POSS composite scaffolds compared to diatomite (0.571) and Si-HAP (0.531) incorporated scaffolds. The differentiation of osteoblast like MG-63 cells in osteogenic media increased the ALP activity, which was supported with the mineralization on the surface at the latest stages of the incubation period. Osteocalcin concentrations of MG-63 cells on scaffolds were depicted in Fig. 13. Results showed that Si-HAP and POSS incorporation enhanced the osteocalcin production for 21 day due to the interaction of these particles with osteoblast like cells at nano-level. However, diatomite incorporation did not show a significant effect compared to control group. This may result from the microstructure of diatomite frustules as silica source and possible fast release of silicon ions from diatomite particles at early incubation periods. Thus, Si release may decrease at 21 and 28 day of incubation. Despite the lower osteocalcin levels, diatomite incorporated scaffolds showed an increment during incubation period. Similarly, Le et al. investigated the silicon release kinetics from diatom particles and indicated that diatomite particles exhibited fast release at early incubation followed by a lower rate with the incubation time [78].

3.7.4. In vitro mineralization with von Kossa and Alizarin Red staining

von Kossa and Alizarin Red S staining methods were performed to observe the calcium and phosphate deposition on the surface which are very important constituents of bone mineralization. Silica incorporated material surface generally affect the biomineralization process by forming calcium silicate bridge for CaP nucleation. The negatively charged Si—O radicals formed by the dissociation of Si-OH groups, interacted electrostatically with the positively charged calcium to form calcium silicate. The calcium silicate interacted with the phosphate ions to form amorphous calcium phosphate, followed by a transformation to crystalline apatite on the material surface [79]. Stereomicroscopy images showed enhanced mineralization on cell-seeded scaffold surfaces with the addition of silica sources to the CS/Na-CMC blend (Fig. 14). Cell-free scaffolds were also stained and observed to indicate the colour difference. However, Si-HAP incorporated cell-free scaffolds observed as colored due to the trace amount of Ca^{2+} and PO_4^{3-} content. The calcium deposition on inorganic phase incorporated scaffolds can be observed with red colored parts due to Alizarin Red S staining. After 14th day of incubation in osteogenic medium, POSS and diatomite incorporated scaffolds induced regional mineral deposition on the surface. Similarly, the brownish colour formation is attributed to phosphate deposition on scaffolds with the von Kossa staining method. The von Kossa staining results of diatomite and POSS composites demonstrated localized and enhanced phosphate deposition on the surface compared to control and Si-HAP incorporated scaffolds. Quantification of Alizarin Red staining also validated the imaging results (Fig. 14). It was observed that POSS and Diatomite incorporation in CS/Na-CMC matrix significantly increased the calcium deposition on scaffolds ($P < 0.05$). Si-HAP loaded scaffolds showed similar results with the control group.

4. Conclusions

In this study, CS/Na-CMC polyelectrolyte scaffolds fabricated successfully with the freeze-drying method. As a well-known inorganic reinforcement, Si-HAP particles were incorporated into CS/Na-CMC scaffolds to compare with the effect of two different novel silica sources. Scaffolds showed a proper pore size and structure for bone regeneration. Addition of natural and synthetic silica particles provided an improvement in mechanical properties and water uptake capacity as well as biological properties. All scaffolds were found to be cytocompatible to MG-63 & SW1353 cells and promoted the differentiation of pre-osteoblast MG-63 cells in osteogenic media and also increased the ALP activity, which was supported with the mineralization on the surfaces. Both Si substituted HAP and POSS nanoparticles enhanced the osteocalcin levels at 21 day due to the altering effect on surface topography and cell bioactivity at nanolevel. Diatomite particles did not have a significant effect on osteocalcin levels, however showed an increasing trend during incubation. Although, porous compact cylindrical microstructure of *Melosira granulata* diatomite frustules provided good interaction with polymer matrix and fast silicate release from structure inducing biomineralization process, desired bioactive effect was not observed due to the possible weak cell-material interaction at microlevel. Hence, it was concluded that diatomite and POSS silica particles can be used as an alternative inorganic reinforcement to mimic the trabecular bone structure and enhance the bioactivity by increasing the biomineralization on biomaterial additionally.

Acknowledgments

This research did not receive any specific grant from funding agencies in the public, commercial, or not-for-profit sectors. The authors thank Center for Materials Research (IZTECH CMR) for SEM analysis and stereomicroscopy imaging. Also, we appreciate Dr. Berivan Erik Cecen and Prof. Dr. Leyla Didem Kozaci for supplying MG-63 and SW1353 cell lines for *in vitro* studies, respectively. This research did not receive any specific grant from funding agencies in the public, commercial, or not-for-profit sectors.

References

[1] W. Wang, X. Sun, L. Huang, Y. Gao, J. Ban, L. Shen, J. Chen, Structure-property relationships in hybrid dental nanocomposite resins containing monofunctional and multifunctional polyhedral oligomeric silsesquioxanes, Int. J. Nanomedicine 9 (1) (2014) 841–852.
[2] R. Jayakumar, D. Menon, K. Manzoor, S.V. Nair, H. Tamura, Biomedical applications of chitin and chitosan based nanomaterials—a short review, Carbohydr. Polym. 82 (2) (2010) 227–232.
[3] J.M. Unagolla, T.E. Alahmadi, A.C. Jayasuriya, Chitosan microparticles based polyelectrolyte complex scaffolds for bone tissue engineering in vitro and effect of calcium phosphate, Carbohydr. Polym. 199 (2018) 426–436.
[4] V. Brar, G. Kaur, Preparation and characterization of polyelectrolyte complexes of *Hibiscus esculentus* (Okra) gum and chitosan, Int. J. Biomater. (2018) 1–7.
[5] L. Jiang, Y. Li, X. Wang, L. Zhang, J. Wen, M. Gong, Preparation and properties of nano-hydroxyapatite/chitosan/carboxymethyl cellulose composite scaffold, Carbohydr. Polym. 74 (3) (2008) 680–684.
[6] N.A. Ramli, T.W. Wong, Sodium carboxymethylcellulose scaffolds and their physicochemical effects on partial thickness wound healing, Int. J. Pharm. 403 (1–2) (2011) 73–82.
[7] X. Chen, J. Liu, Z. Feng, Z. Shao, Macroporous chitosan/carboxymethylcellulose blend membranes and their application for lysozyme adsorption, J. Appl. Polym. Sci. 96 (4) (2005) 1267–1274.
[8] Q. Zhao, J. Qian, Q. An, C. Gao, Z. Gui, H. Jin, Synthesis and characterization of soluble chitosan/sodium carboxymethyl cellulose polyelectrolyte complexes and the pervaporation dehydration of their homogeneous membranes, J. Membr. Sci. 333 (1–2) (2009) 68–78.
[9] H. Chen, M. Fan, Chitosan/carboxymethyl cellulose polyelectrolyte complex scaffolds for pulp cells regeneration, J. Bioact. Compat. Polym. 22 (5) (2007) 475–491.
[10] T. Hasan, A. Nurhan, Carboxymethyl cellulose from sugar beet pulp cellulose as a hydrophilic polymer in coating of mandarin, J. Food Eng. 62 (2004) 271–279.
[11] J. Liuyun, L. Yubao, X. Chengdong, A novel composite membrane of chitosan-carboxymethyl cellulose polyelectrolyte complex membrane filled with nano-hydroxyapatite I, Preparation and properties, Journal of Materials Science: Materials in Medicine 20 (8) (2009) 1645–1652.
[12] X.J. Tang, L. Gui, X.Y. Lü, Hard tissue compatibility of natural hydroxyapatite/chitosan composite, Biomed. Mater. 3 (4) (2008) 044115.
[13] J.C. Fricain, S. Schlaubitz, C. Le Visage, I. Arnault, S.M. Derkaoui, R. Siadous, S. Catros, C. Lalande, R. Bareille, M. Renard, T. Fabre, S. Cornet, M. Durand, A. Leonard, N. Sahraoui, D. Letourneur, J. Amedee, A nano-hydroxyapatite–pullulan/dextran polysaccharide composite macroporous material for bone tissue engineering, Biomaterials 34 (12) (2013) 2947–2959.
[14] S.M. Park, H.S. Kim, Preparation of acetylated chitosan/carbonated hydroxyapatite composite barriers for guided bone regeneration, Macromol. Res. 25 (2) (2017) 158–164.
[15] E. Sachlos, D. Gotora, J.T. Czernuszka, Collagen scaffolds reinforced with biomimetic composite nano-sized carbonate-substituted hydroxyapatite crystals and shaped by rapid prototyping to contain internal microchannels, Tissue Eng. 12 (9) (2006) 2479–2487.
[16] S. Zhang, Hydroxyapatite Coatings for Biomedical Applications, CRC Press, Florida, USA, 2013.
[17] E.S. Thian, J. Huang, S.M. Best, Z.H. Barber, W. Bonfield, A new way of incorporating silicon in hydroxyapatite (Si-HA) as thin films, J. Mater. Sci. Mater. Med. 16 (5) (2005) 411–415.
[18] K.B. Narayanan, N. Sakthivel, Green synthesis of biogenic metal nanoparticles by terrestrial and aquatic phototrophic and heterotrophic eukaryotes and biocompatible agents, Adv. Colloid Interf. Sci. 169 (2) (2011) 59–79.
[19] K. Madhumathi, P.S. Kumar, K.C. Kavya, T. Furuike, H. Tamura, S.V. Nair, R. Jayakumar, Novel chitin/nanosilica composite scaffolds for bone tissue engineering applications, Int. J. Biol. Macromol. 45 (3) (2009) 289–292.
[20] V. Puchol, J. El Haskouri, J. Latorre, C. Guillem, A. Beltrán, D. Beltran, P. Amoros, Biomimetic chitosan-mediated synthesis in heterogeneous phase of bulk and mesoporous silica nanoparticles, Chem. Commun. 19 (2009) 2694–2696.
[21] C.J. Wu, A.K. Gaharwar, P.J. Schexnailder, G. Schmidt, Development of biomedical polymer-silicate nanocomposites: a materials science perspective, Materials 3 (5) (2010) 2986–3005.
[22] C.U. Pittman, G.Z. Li, H.S. Cho, Chemical bonding between phenolic resins and polyhedral oligomeric silsesquioxanes (POSS) in inorganic–organic hybrid nanocomposites, J. Inorg. Organomet. Polym. Mater. 16 (1) (2006) 43–59.
[23] D. Xu, L.S. Loo, K. Wang, Characterization and diffusion behavior of chitosan–POSS composite membranes, J. Appl. Polym. Sci. 122 (1) (2011) 427–435.
[24] Z. Hong, R.L. Reis, J.F. Mano, Preparation and in vitro characterization of scaffolds of poly (L-lactic acid) containing bioactive glass ceramic nanoparticles, Acta Biomater. 4 (5) (2008) 1297–1306.
[25] N.M. Sulca, A. Lungu, S.A. Garea, H. Iovu, Monitoring the synthesis of new polymer nanocomposites based on different polyhedral oligomeric silsesquioxanes using Raman spectroscopy, J. Raman Spectrosc. 40 (11) (2009) 1634–1640.
[26] S. Tamburaci, F. Tihminlioglu, Novel POSS reinforced chitosan composite membranes for guided bone tissue regeneration, J. Mater. Sci. Mater. Med. 29 (1) (2018) 1.
[27] H. Ghanbari, S.M. Marashi, Y. Rafiei, K. Chaloupka, A.M. Seifalian, Biomedical application of polyhedral oligomeric silsesquioxane nanoparticles, applications of polyhedral oligomeric silsesquioxanes, Adv. Silicon Sci. 3 (2011) 363–399.
[28] C. McCusker, J.B. Carroll, V.M. Rotello, Cationic polyhedral oligomeric silsesquioxane (POSS) units as carriers for drug delivery processes, Chem. Commun. 8 (2005) 996–998.
[29] R.Y. Kannan, H.J. Salacinski, J. De Groot, I. Clatworthy, L. Bozec, M. Horton, P.E. Butler, A.M. Seifalian, The antithrombogenic potential of a polyhedral oligomeric silsesquioxane (POSS) nanocomposite, Biomacromolecules 7 (1) (2006) 215–223.
[30] P.T. Knight, K.M. Lee, H. Qin, P.T. Mather, Biodegradable thermoplastic polyurethanes incorporating polyhedral oligosilsesquioxane, Biomacromolecules 9 (9) (2008) 2458–2467.
[31] H. Dodiuk-Kenig, Y. Maoz, K. Lizenboim, I. Eppelbaum, B. Zalsman, S. Kenig, The effect of grafted caged silica (polyhedral oligomeric silesquioxanes) on the properties of dental composites and adhesives, J. Adhes. Sci. Technol. 20 (12) (2006) 1401–1412.
[32] S.K. Kim, S.J. Heo, J.Y. Koak, J.H. Lee, Y.M. Lee, D.J. Chung, J.I. Lee, S.D. Kong, A biocompatibility study of a reinforced acrylic-based hybrid denture composite resin with polyhedral oligosilsesquioxane, J. Oral Rehabil. 34 (5) (2007) 389–395.
[33] E. Gültürk, M. Güden, Thermal and acid treatment of diatom frustules, J. Achiev. Mater. Manuf. Eng. 46 (2011) 196–203.
[34] K.M. Wee, T.N. Rogers, B.S. Altan, S.A. Hackney, C. Hamm, Engineering and medical applications of diatoms, J. Nanosci. Nanotechnol. 5 (1) (2005) 88–91.
[35] Y. Wang, J. Cai, Y. Jiang, X. Jiang, D. Zhang, Preparation of biosilica structures from frustules of diatoms and their applications: current state and perspectives, Appl. Microbiol. Biotechnol. 97 (2) (2013) 453–460.
[36] M. Lopez-Alvarez, E.L. Solla, P. González, J. Serra, B. Leon, A.P. Marques, R.L. Reis, Silicon–hydroxyapatite bioactive coatings (Si–HA) from diatomaceous earth and silica. Study of adhesion and proliferation of osteoblast-like cells, J. Mater. Sci. Mater. Med. 20 (5) (2009) 1131–1136.
[37] A. Hertz, V. FitzGerald, E. Pignotti, J.C. Knowles, T. Sen, I.J. Bruce, Preparation and characterisation of porous silica and silica/titania monoliths for potential use in bone replacement, Microporous Mesoporous Mater. 156 (2012) 51–61.
[38] I. Rea, M. Terracciano, L. De Stefano, Synthetic vs natural: diatoms bioderived porous materials for the next generation of healthcare nanodevices, Adv. Healthcare Mater. 6 (3) (2017) 1601125.
[39] P.J. Walsh, S.A. Clarke, M. Julius, P.B. Messersmith, Exploratory testing of diatom silica to map the role of material attributes on cell fate, Sci. Rep. 7 (1) (2017) 14138.
[40] S. Tamburaci, F. Tihminlioglu, Diatomite reinforced chitosan composite membrane

as potential scaffold for guided bone regeneration, Mater. Sci. Eng. C 80 (2017) 222–231.
[41] R. Zhang, P.X. Ma, Poly (α-hydroxyl acids)/hydroxyapatite porous composites for bone-tissue engineering. I. Preparation and morphology, J. Biomed. Mater. Res. 44 (4) (1999) 446.
[42] H. Puchtler, S.N. Meloan, M.S. Terry, On the history and mechanism of alizarin and alizarin red S stains for calcium, J. Histochem. Cytochem. 17 (2) (1969) 110–124.
[43] C.A. Gregory, W.G. Gunn, A. Peister, D.J. Prockop, An Alizarin red-based assay of mineralization by adherent cells in culture: comparison with cetylpyridinium chloride extraction, Anal. Biochem. 329 (1) (2004) 77–84.
[44] L. John, Selected developments and medical applications of organic–inorganic hybrid biomaterials based on functionalized spherosilicates, Mater. Sci. Eng. C 88 (2018) 172–181.
[45] S.W. Ha, M. Viggeswarapu, M.M. Habib, G.R. Beck Jr., Bioactive effects of silica nanoparticles on bone cells are size, surface, and composition dependent, Acta biomaterialia 82 (2018) 184–196.
[46] G. Li, L. Wang, H. Ni, C.U. Pittman, Polyhedral oligomeric silsesquioxane (POSS) polymers and copolymers: a review, J. Inorg. Organomet. Polym. 11 (3) (2001) 123–154.
[47] K. Whang, C.H. Thomas, K.E. Healy, G. Nuber, A novel method to fabricate bioabsorbable scaffolds, Polymer 36 (4) (1995) 837–842.
[48] S.F. Hulbert, F.A. Young, R.S. Mathews, J.J. Klawitter, C.D. Talbert, F.H. Stelling, Potential of ceramic materials as permanently implantable skeletal prostheses, J. Biomed. Mater. Res. 4 (3) (1970) 433–456.
[49] C.M. Murphy, M.G. Haugh, F.J. O'Brien, The effect of mean pore size on cell attachment, proliferation and migration in collagen–glycosaminoglycan scaffolds for bone tissue engineering, Biomaterials 31 (3) (2010) 461–466.
[50] A.R. Costa-Pinto, R.L. Reis, N.M. Neves, Scaffolds based bone tissue engineering: the role of chitosan, Tissue Eng. B Rev. 17 (5) (2011) 331–347.
[51] S.H. Phillips, T.S. Haddad, S.J. Tomczak, Developments in nanoscience: polyhedral oligomeric silsesquioxane (POSS)-polymers, Curr. Opinion Solid State Mater. Sci. 8 (1) (2004) 21–29.
[52] B.D. Cullity (Ed.), Elements of X-ray Diffraction, Second ed., Addison-Wesley Publishing Co, Reading, MA, 1978, p. 101.
[53] V.M. Rusu, C.H. Ng, M. Wilke, B. Tiersch, P. Fratzl, M.G. Peter, Size-controlled hydroxyapatite nanoparticles as self-organized organic–inorganic composite materials, Biomaterials 26 (26) (2005) 5414–5426.
[54] Y. Zhao, D.A. Schiraldi, Thermal and mechanical properties of polyhedral oligomeric silsesquioxane (POSS)/polycarbonate composites, Polymer 46 (25) (2005) 11640–11647.
[55] B.S. Kim, P.T. Mather, Morphology, microstructure, and rheology of amphiphilic telechelics incorporating polyhedral oligosilsesquioxane, Macromolecules 39 (26) (2006) 9253–9260.
[56] L. Liu, Y. Hu, L. Song, X. Gu, Z. Ni, Fabrication of lamellar nanostructure from cage-like poly-anion silicate and surfactant by template-directed synthesis, J. Compos. Mater. 45 (3) (2011) 307–319.
[57] D.B. Cordes, P.D. Lickiss, F. Rataboul, Recent developments in the chemistry of cubic polyhedral oligosilsesquioxanes, Chem. Rev. 110 (4) (2010) 2081–2173.
[58] N. Jalarvo, O. Gourdon, G. Ehlers, M. Tyagi, S.K. Kumar, K.D. Dobbs, R.J. Smalley, W.E. Guise, A. Ramirez-Cuesta, C. Wildgruber, M.K. Crawford, Structure and dynamics of octamethyl-POSS nanoparticles, J. Phys. Chem. C 118 (10) (2014) 5579–5592.
[59] E.A. Gültürk, M. Güden, A. Taşdemirci, Calcined and natural frustules filled epoxy matrices: the effect of volume fraction on the tensile and compression behaviour, Compos. Part B 44 (1) (2013) 491–500.
[60] H. Itagaki, M. Tokai, T. Kondo, Physical gelation process for cellulose whose hydroxyl groups are regioselectively substituted by fluorescent groups, Polymer 38 (16) (1997) 4201–4205.
[61] C. Rosca, M.I. Popa, G. Lisa, G.C. Chitanu, Interaction of chitosan with natural or synthetic anionic polyelectrolytes. 1. The chitosan–carboxymethylcellulose complex, Carbohydr. Polym. 62 (1) (2005) 35–41.
[62] L. Liu, X. Xu, Polystyrene nanocomposites with improved combustion properties by using TMA-POSS and organic clay, J. Therm. Anal. Calorim. 124 (2) (2016) 743–749.
[63] J.A. Sowjanya, J. Singh, T. Mohita, S. Sarvanan, A. Moorthi, N. Srinivasan, N. Selvamurugan, Biocomposite scaffolds containing chitosan/alginate/nano-silica for bone tissue engineering, Colloids Surf. B: Biointerfaces 109 (2013) 294–300.
[64] M. Kharaziha, M.H. Fathi, H. Edris, Development of novel aligned nanofibrous composite membranes for guided bone regeneration, J. Mech. Behav. Biomed. Mater. 24 (2013) 9–20.
[65] M. Dziadek, E. Stodolak-Zych, K. Cholewa-Kowalska, Biodegradable ceramic-polymer composites for biomedical applications: a review, Mater. Sci. Eng. C 71 (2017) 1175–1191.
[66] R. Hill, An alternative view of the degradation of bioglass, J. Mater. Sci. Lett. 15 (13) (1996) 1122–1125.
[67] R. Viitala, M. Jokinen, J.B. Rosenholm, Mechanistic studies on release of large and small molecules from biodegradable SiO_2, Int. J. Pharm. 336 (2) (2007) 382–390.
[68] T.D.H. Le, W. Bonani, G. Speranza, V. Sglavo, R. Ceccato, D. Maniglio, A. Motta, C. Migliaresi, Processing and characterization of diatom nanoparticles and microparticles as potential source of silicon for bone tissue engineering, Mater. Sci. Eng. C 59 (2016) 471–479.
[69] A.E. Porter, N. Patel, J.N. Skepper, S.M. Best, W. Bonfield, Effect of sintered silicate-substituted hydroxyapatite on remodelling processes at the bone–implant interface, Biomaterials 25 (16) (2004) 3303–3314.
[70] K.C. Kavya, R. Jayakumar, S. Nair, K.P. Chennazhi, Fabrication and characterization of chitosan/gelatin/nSiO_2 composite scaffold for bone tissue engineering, Int. J. Biol. Macromol. 59 (2012) 255–263.
[71] H. Yang, C. Liu, D. Yang, H. Zhang, Z. Xi, Comparative study of cytotoxicity, oxidative stress and genotoxicity induced by four typical nanomaterials: the role of particle size, shape and composition, J. Appl. Toxicol. 29 (1) (2009) 69–78.
[72] E.E. Golub, K. Boesze-Battaglia, The role of alkaline phosphatase in mineralization, Curr. Opin. Orthop. 18 (5) (2007) 444–448.
[73] A. Rutkovskiy, K.O. Stensløkken, I.J. Vaage, Osteoblast differentiation at a glance, Med. Sci. Monit. Basic Res. 22 (2016) 95.
[74] G.R. Beck, S.W. Ha, C.E. Camalier, M. Yamaguchi, Y. Li, J.K. Lee, M.N. Weitzmann, Bioactive silica-based nanoparticles stimulate bone-forming osteoblasts, suppress bone-resorbing osteoclasts, and enhance bone mineral density in vivo, nanomedicine nanotechnology, Biol. Med. 8 (6) (2012) 793–803.
[75] K. Madhumathi, P.T. Sudheesh Kumar, K.C. Kavya, T. Furuike, H. Tamura, S.V. Nair, R. Jayakumar, Novel chitin/nanosilica composite scaffolds for bone tissue engineering applications, Int. J. Biol. Macromol. 45 (3) (2009) 289–292.
[76] V. Puchol, J. El Haskouri, J. Latorre, C. Guillem, A. Beltrán, D. Beltrán, P. Amorós, Biomimetic chitosan-mediated synthesis in heterogeneous phase of bulk and mesoporous silica nanoparticles, Chem. Commun. 19 (2009) 2694–2696.
[77] C.J. Wu, A.K. Gaharwar, P.J. Schexnailder, G. Schmidt, Development of biomedical polymer-silicate nanocomposites: a materials science perspective, Materials 3 (5) (2010) 2986–3005.
[78] Thi Duy Hanh Le, et al., Processing and characterization of diatom nanoparticles and microparticles as potential source of silicon for bone tissue engineering, Mater. Sci. Eng. C 59 (2016) 471–479.
[79] M. Tanahashi, T. Yao, T. Kokubo, M. Minoda, T. Miyamoto, T. Nakamura, T. Yamamuro, Apatite coated on organic polymers by biomimetic process: improvement in its adhesion to substrate by NaOH treatment, J. Appl. Biomater. 5 (4) (1994) 339–347.